Ultrasonic Characterization of Crack-Like Defects Using Scattering Matrix Similarity Metrics

Long Bai, Alexander Velichko, and Bruce W. Drinkwater

***Abstract*—Crack-like defects form an important type of target defect in nondestructive evaluation, and accurately characterizing them remains a challenge, particularly for small cracks and inclined cracks. In this paper, scattering matrices are used for defect characterization through use of the correlation coefficient and the structural similarity (SSIM) index as similarity metrics. A set of reference cracks that have different lengths and orientation angles are compared with the test defect and the best match is determined in terms of the maximum similarity score between the scattering matrices of the test defect and reference cracks. Defect characterization using similarity metrics is invariant to scale and shift, so calibration of experimental data is not needed. Principal component analysis (PCA) is adopted to reduce the effect of measurement noise and recover the original shape of scattering matrices from noisy data. The performance of the proposed algorithm is studied in both simulation and experiments. The length and orientation angle of four different test cracks are measured at two different noise levels in the simulation case, and excellent agreement is achieved between the measurement results and the actual values. Experimentally, the lengths of five subwavelength cracks are measured to within 0.10 mm, and their orientation angles are measured to within 5°.**

I. Introduction

Crack-like defects form an important type of target defect in nondestructive evaluation [1]. Accurate characterization of crack-like defects leads to more quantitative monitoring of the structures being inspected, providing essential information on the integrity of the structure. For example, the depth of surface breaking cracks was measured by the potential drop method, which relates the potential drop to the crack length and the crack depth [2]. Model-based estimation of ultrasonic signal parameters (e.g., the time of arrival) was proposed in [3]–[5], and cracks were sized by the difference in arrival times between the tip-diffracted and corner-trap echoes.

In recent years, ultrasonic arrays have seen increased use for defect detection and characterization because of their ability to form an image of the interior of the test structure [6]. For example, the total focusing method (TFM) [7] works by postprocessing the full set of array data that consists of measurements from all transmitter–receiver pairs in an array. By focusing the ultrasonic beam at each pixel point in the region of interest, the TFM can produce acoustic images of significantly higher resolution than conventional plane and focused B-scan images [8], [9]. The inverse wave field extrapolation [10] and the wavenumber algorithms [11] work under the same scheme (i.e., processing the full array data and synthetically focusing the beam at each image pixel), and provide resolving capabilities similar to TFM. As a result, for relatively large cracks, the parameters of crack length and orientation angle can be extracted directly from these high-resolution images (e.g., by fitting a box that covers all of the pixels within −6 dB of its maximum amplitude [12]). The performance of this so-called −6-dB box fitting approach was also studied with application to rough cracks [13], and it was shown that such image-based sizing tends to underestimate the length of inclined cracks with high roughness [13]. Imaged-based sizing algorithms require the target crack to be sufficiently large, and hence perform poorly when the crack length becomes comparable with the wavelength.

The scattered field from a crack is known to encode the key information about the crack [1], such as location, size, and orientation angle. The interaction of an ultrasonic wave with cracks can be modeled analytically if they are assumed to have simple geometry: elliptical cracks [14], planar cracks [15], penny-shaped cracks and spherical cavities [16], and surface-breaking cracks [17]. The scattering matrix describes the scattered field of a defect (in the far field) as a function of incident and scattered angles as well as frequency [12]. Scattering matrices of side-drilled holes were estimated by an exact model (based on the separation of variables method) and the Kirchhoff model, and used to accurately predict the ultrasonic array data [18]. The vector TFM (VTFM) [19] extracts vector information from the scattering matrix [12], [20] for each pixel point in the image, which can be used to characterize the defect as planar or volumetric. With the VTFM results, the orientation angle of 1-mm cracks (i.e., approximately one ultrasonic wavelength in length) was determined within 5°, and cracks were distinguished from side-drilled holes. Scattering matrices were also used to size small cracks, and the length of cracks was related to the maximum amplitude [20] or the half-width at half-maximum (HWHM) of the pulse–echo part of the scattering matrix [12]. For experi-

Manuscript received November 13, 2014; accepted December 11, 2014. This work was supported through the core research program within the UK Research Centre in NDE (RCNDE) funded by the Engineering and Physical Sciences Research Council (EPSRC; grant number EP/L022125/1).

The authors are with the Department of Mechanical Engineering, University of Bristol, Bristol, UK (e-mail: lb13340@bristol.ac.uk).

DOI http://dx.doi.org/10.1109/TUFFC.2014.006848

mental measurements, a reference scatterer, for which the scattering matrix is exactly known, is needed to normalize the absolute amplitudes of the extracted scattering matrices when amplitude-based sizing is used [20]. Because the HWHM is only related to the shape of a scattering matrix, HWHM-based characterization does not require such calibration of experimental data. However, HWHM-based characterization has two limitations. First, the HWHM can only be correctly measured when the specular reflection is included in the scattering matrix, and thus is not applicable for certain cases (e.g., vertical cracks). Second, the performance of HWHM-based sizing degrades dramatically with the presence of measurement noise, as shown in this paper.

In this paper, an approach that outperforms the existing HWHM-based characterization is proposed. The robustness of the method to noise is improved by the application of principal component analysis (PCA) [21]. Two similarity metrics are introduced in Sections II and III, and are used to find best match results based on the shape of scattering matrices. The performance of the proposed approach is studied both with simulated data (in Section III) and experimentally (in Section IV).

II. Characterization Based on Noise-Free Scattering Matrices

A. Preparation of the Database

This paper studies the characterization of small cracks, and as such, all of the cracks considered have a length comparable to or less than one wavelength. Given the scattering matrix of a test defect, the first step of the proposed approach is to form the database using the scattering matrices of reference cracks. In this paper, the scattering matrices of cracks are simulated using the 2-D fast semi-analytical technique developed in [22], which is based on a boundary integral equation method, and only the longitudinal-longitudinal (LL) scattering matrix is output, although the model inherently includes all modes. According to this method, the crack opening displacements are calculated first and then an exact integral representation of the scattered wave field [23] is used to calculate the scattering matrix. Because of the limited aperture of an array, practically extracted scattering matrices are often only a portion of the global scattering matrix [i.e., the ranges of incident (θ_1) and scattering (θ_2) angles are limited, instead of ranging from $-\pi$ to π], and the incident and scattering angles that can be obtained with a specific array are determined by array element positions and the position and angle of the crack. Fig. 1 shows the geometry of the measurement configuration, from which the scattering matrices of test and reference cracks are extracted. The example linear array adopted here and in the following experimental case has 64 elements, and the operation frequency of the array is 5 MHz. Detailed array parameters are given in Table I. If a horizontal crack is considered, it is easy to see that the incident and scattering angles of the extracted scattering matrix will be limited to $[\varphi_1, \varphi_2]$. (Note that φ_1 has a negative value because it is measured anticlockwise from the z-axis.) Similarly, the scattering matrix of the inclined crack will include incident and scattering angles ranging from $\varphi_1 - \alpha$ to $\varphi_2 - \alpha$. Note that the orientation angle α of the crack can have either positive (if measured clockwise) or negative (if measured anticlockwise) values.

TABLE I. Array Parameters for Simulation and Experimental Measurements.

Array parameter	Value
Number of elements	64
Elements width (mm)	0.53
Element pitch (mm)	0.63
Element length (mm)	15
Central frequency (MHz)	5
Bandwidth (−6 dB) (MHz)	3–7

Figs. 2(a)–2(d) show the scattering matrices (calculated by the semi-analytical technique and extracted from the configuration shown in Fig. 1) of the four different test cracks A–D. In this work, only the amplitude of the scattering matrix has been considered, and hereafter the term "scattering matrix" refers to the amplitude of the scattering matrix. The material in Fig. 1 is assumed to be aluminum, with Young's modulus = 69 GPa, Poisson's ratio = 0.334, and density = 2700 kg·m^{-3}. The length and orientation angle of each crack are specified in Table II. Because the ultrasonic wavelength in aluminum is 1.24 mm when the frequency is 5 MHz, the length of cracks C and D is comparable to one wavelength, whereas the lengths of cracks A and B are below one wavelength. The database is then formed by the scattering matrices of a set of reference cracks, which have lengths ranging from 0.2 mm to 2 mm (at 0.05 mm intervals), and orientation angles $\alpha = -85°$ to 90° (at 5° intervals). This is chosen to cover the crack sizes and orientation angles of interest.

If the angular range of the scattering matrix includes the specular reflection, the HWHM can be measured from the pulse–echo component of the scattering matrix (i.e., where the incident and scattering angles are identical) as shown in Figs. 3(a) and 3(b). Because the HWHM de-

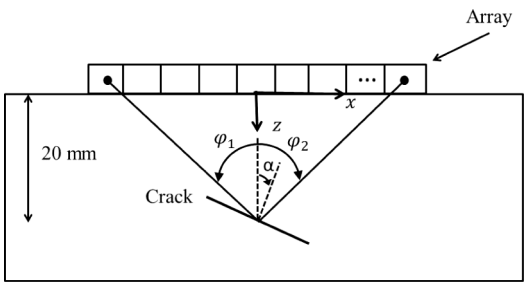

Fig. 1. Geometry of the scattering matrix measurement.

TABLE II. DETAILS OF CRACKS A–D.

Crack	Length (mm)	Orientation angle α (°)
A	1.00	0
B	0.50	30
C	1.20	90
D	1.20	−70

creases monotonically as crack size increases [12], the relationship between crack size and the HWHM was established (see [12, Fig. 6(c)]), making it possible to size cracks based on their scattering matrices. In addition, the orientation angles of test cracks were found to be the angle corresponding to the maximum amplitude of the pulse–echo signal. HWHM-based characterization is applied to the scattering matrices of test cracks and the results are given in Fig. 3. In Fig. 3(a), the full-width at half-maximum (FWHM) is measured, and the result of crack A is obtained as 1.01 mm, 1°, which is in excellent agreement with the true value shown in Table II. Only the half-width at half-maximum is measured in Fig. 3(b), and crack B is characterized as 0.50 mm, 30°. It seems that HWHM-based characterization works well for cracks A and B. However, HWHM-based characterization fails to give a measurement result for crack C because the peak of the scattering matrix cannot be identified within the measured angular range [see Fig. 3(c)]. Furthermore, the characterization result of crack D is 1.07 mm, −25°, which is very poor. This is because the peak identified here is not the specular reflection.

B. The Correlation Coefficient as a Similarity Metric

Once the scattering matrix of a test crack is obtained, this can be compared with the set of reference (i.e., the database) cracks, and the one that is the best match to the test crack can be determined. In this paper, the best match is found in terms of the maximum similarity score between the scattering matrices of the test crack and reference cracks. Evaluation of the similarity between two images has been extensively studied in image registration [24], and various similarity (or dissimilarity) measures were introduced in [25], including similarity measures such as the Pearson correlation coefficient [26], Spearman's rank correlation coefficient (Spearman's rho) [27], Kendall rank correlation coefficient (Kendall's tau) [28], and mutual information [29] and dissimilarity measures, such as the sum of absolute differences (L_1 norm) and the sum of squared differences (square L_2 norm). The calculation of Spearman's rho and Kendall's tau is based on ranks of the intensities, and mutual information requires the joint probabilities of the corresponding intensities [25]. Here, the correlation coefficient which uses the normalized intensities is selected as the first similarity metric to be explored for the following reasons: First, popular dissimilarity (distance) metrics such as L_1 norm and square L_2 norm calculate the differences between the corresponding pixel

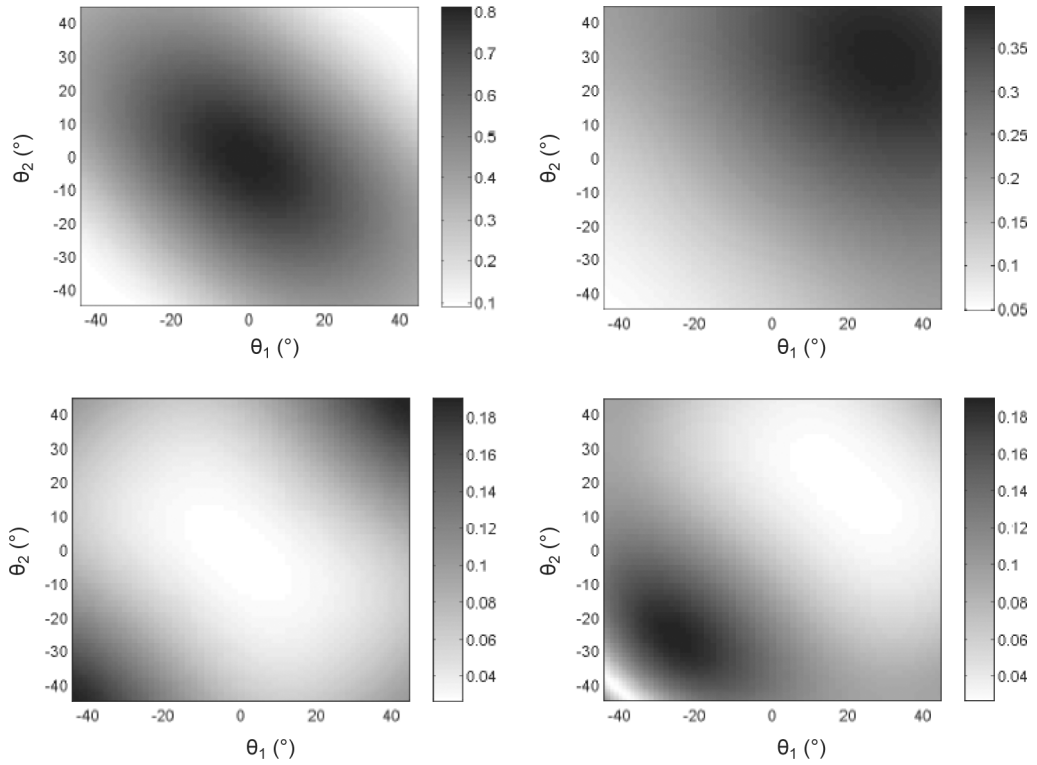

Fig. 2. Scattering matrices (calculated by the semi-analytical technique [22], and extracted from the configuration shown in Fig. 1) of the test cracks, where (a)–(d) are the scattering matrices of cracks A–D, respectively. The scattering matrix describes the scattered field of a defect (in the far field) as a function of incident (θ_1) and scattered (θ_2) angles as well as frequency, and here the amplitude of the scattering matrices is plotted. The length and orientation angle of each crack are specified in Table II.

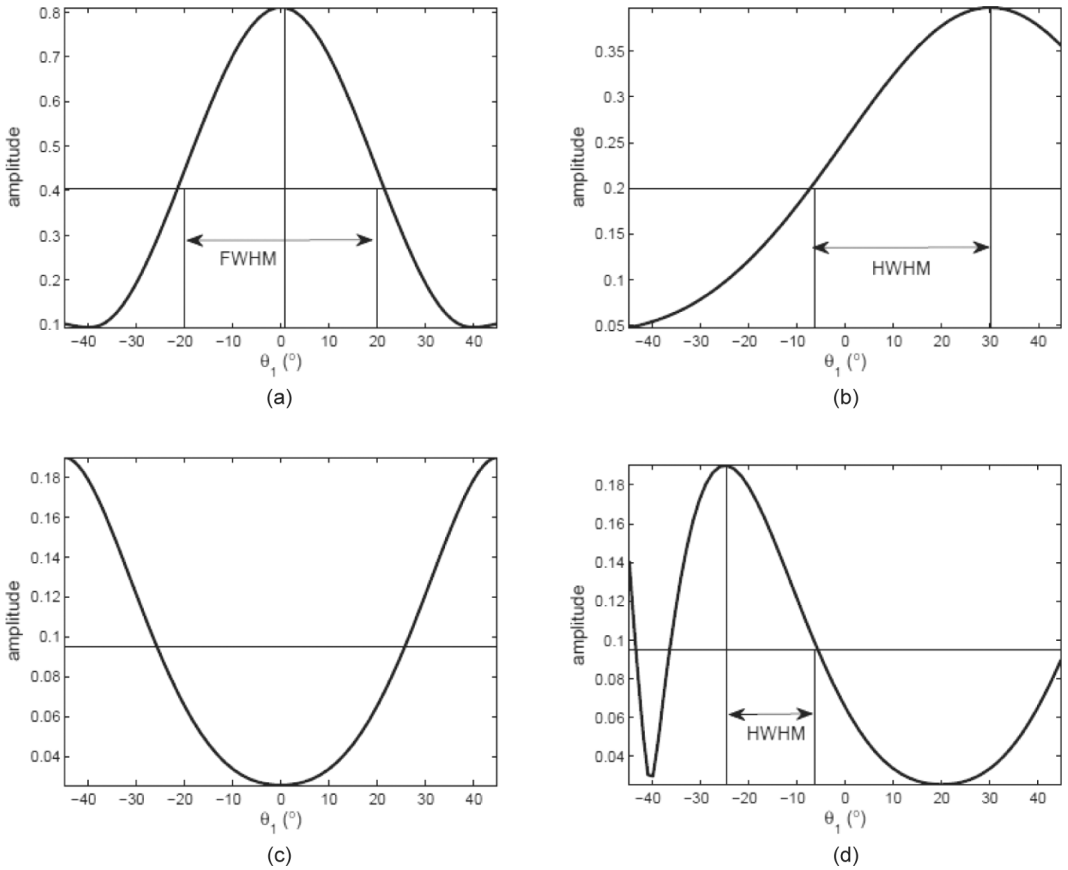

Fig. 3. HWHM-based characterization of the test cracks, where (a)–(d) show the measurements of cracks A–D, respectively. For cracks A and B, the results are 1.01 mm, 1°, and 0.50 mm, 30°, which are in good agreement with reality. For crack C, HWHM-based characterization fails to give a measurement result, and the result of crack D is poor.

intensities of two images, which implies that calibration of experimental data is needed for scattering matrices of test defects to be compared with the reference cracks. On the other hand, as in the HWHM-based characterization, such calibration is not necessary for the calculation of the correlation coefficient. Second, compared with feature-based similarity metrics [30], intensity-based similarity metrics [30] (e.g., the correlation coefficient) are preferred in this paper because it is difficult to tell in advance which features of a scattering matrix are meaningful and should be specifically detected and used for comparison. In fact, the intensity-based similarity metrics merge the feature detection step and the matching step of the image registration [31], and can hence be operated in an automatic way [30]. Moreover, as a widely used similarity measure [30], the correlation coefficient is the optimal criterion for two images obtained with the same modality, when a linear relation is assumed between the signal intensities [32].

For scattering matrices $\mathbf{S}_{\mathrm{E}}$ (obtained experimentally) and $\mathbf{S}_{\mathrm{R}}$ (reference), the correlation coefficient is given by

$$r = \frac{\sum_{i=1}^{N}\sum_{j=1}^{N}(\mathbf{S}_{\mathrm{E}}(i,j)-\overline{\mathbf{S}}_{\mathrm{E}})(\mathbf{S}_{\mathrm{R}}(i,j)-\overline{\mathbf{S}}_{\mathrm{R}})}{\sqrt{\left(\sum_{i=1}^{N}\sum_{j=1}^{N}(\mathbf{S}_{\mathrm{E}}(i,j)-\overline{\mathbf{S}}_{\mathrm{E}})^2\right)\left(\sum_{i=1}^{N}\sum_{j=1}^{N}(\mathbf{S}_{\mathrm{R}}(i,j)-\overline{\mathbf{S}}_{\mathrm{R}})^2\right)}}, \quad (1)$$

where $\mathbf{S}_{\mathrm{E}}$ and $\mathbf{S}_{\mathrm{R}}$ are of size $N \times N$, and $\overline{\mathbf{S}}_{\mathrm{E}}$ and $\overline{\mathbf{S}}_{\mathrm{R}}$ are the mean values of the matrices $\mathbf{S}_{\mathrm{E}}$ and $\mathbf{S}_{\mathrm{R}}$, respectively. Given the test scattering matrix $\mathbf{S}_{\mathrm{E}}$, the correlation coefficients between $\mathbf{S}_{\mathrm{E}}$ and those of the reference cracks ($\mathbf{S}_{\mathrm{R}}$) are calculated. Then, the defect is characterized as the one with which $\mathbf{S}_{\mathrm{E}}$ has the maximum correlation coefficient. Figs. 4(a)–4(d) show the correlation coefficients calculated between the reference cracks and cracks A–D, respectively. It can be seen that there is a peak (maximum) in each figure which corresponds to the actual crack length and orientation angle. It is also clear that the correlation coefficient is more sensitive to the change of orientation angle than the change of crack length. Nevertheless, the correlation coefficient is still able to distinguish between cracks of the same orientation angle.

III. Characterization Based on Scattering Matrices With Noise

A. Scattering Matrices With Noise

It was shown in Fig. 4 that noise-free cracks can be correctly characterized using the correlation coefficient metric. However, for practical measurements, the extraction of the scattering matrix from array data will be inevitably

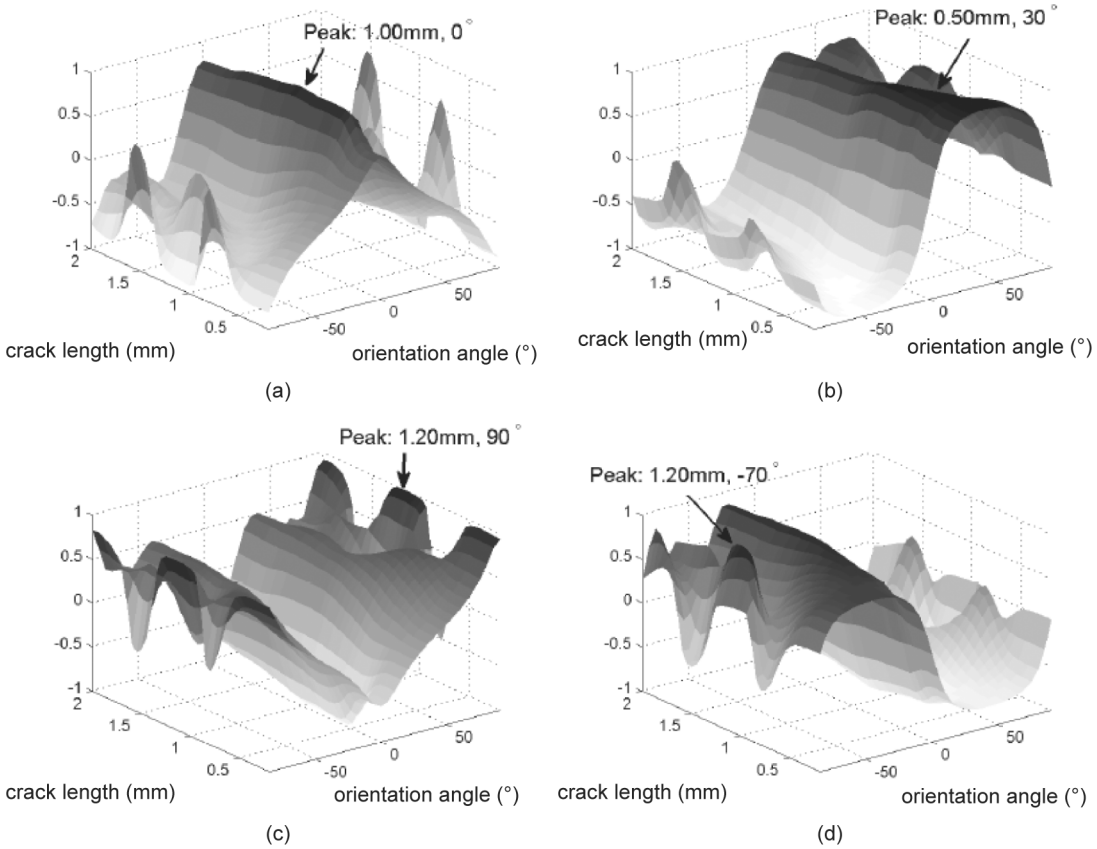

Fig. 4. The correlation coefficients calculated between the scattering matrices of database cracks and the test cracks, where (a)–(d) show the results of cracks A–D, respectively. In each figure, the length and orientation angle corresponding to the peak is indicated with an arrow.

affected by measurement noise. Figs. 5(a) and 5(b) show the scattering matrices of cracks B and D, respectively, with 20% zero-mean random Gaussian measurement added noise. Gaussian noise is added directly to the scattering matrices to simulate measurement noise that would be included in the array data. The relative noise level n_σ is defined with respect to the peak amplitude A_{P} of the scattering matrix of crack A:

$$n_\sigma = \frac{W_\sigma}{A_{\mathrm{P}}} \times 100\%, \tag{2}$$

where W_σ represents the standard deviation of the random noise. HWHM-based characterization results of such scattering matrices with noise are given in Table III. Each measured length and angle in Table III is calculated from 100 realizations of random noise, and shows a spread of two standard deviations from the mean. For a specific realization of noise, if the errors in the measured length and orientation angle are within 0.10 mm and 5°, respectively, then the measurement result is regarded as acceptable. The acceptable result rate is then defined as

$$r_{\mathrm{a}} = \frac{\text{number of acceptable measurements}}{\text{number of total measurements}} \times 100\%. \tag{3}$$

It can be seen from Table III that crack A can be characterized with reasonable accuracy when the noise level is 10%, and the result is degraded when the noise level becomes 20%, which is indicated by the increased standard deviation and the decreased acceptable result rate. For crack B, only the measured orientation angle appears meaningful, but the measurement uncertainty (standard deviation) has increased compared with crack A. For cracks C and D, the results are dominated by the noise.

B. Denoising by Principal Component Analysis

Faced with the difficulty in the characterization of scattering matrices with noise, principal component analysis [21] is adopted in this paper to recover the shape of the original scattering matrices from noisy data. Let $\mathbf{L} \in \mathrm{R}^{N^2 \times M}$ be the database (M is the number of reference cracks in the database), whose columns are the vectorized scattering matrices of the reference cracks. Standardization of $\mathbf{L}$ gives $\mathbf{L}'$, which has the same size as $\mathbf{L}$. The columns of $\mathbf{L}'$ are centered and scaled to have zero mean and unit standard deviation. The mean of the column vectors of $\mathbf{L}'$ is

$$\overline{\mathbf{l}} = \frac{1}{M}\sum_{k=1}^{M} \mathbf{l}_k', \tag{4}$$

where $\mathbf{l}_k'$ is the kth column of the matrix $\mathbf{L}'$. Then the covariance matrix can be calculated as

TABLE III. HWHM-Based Characterization Results of Cracks A-D With Noise.

	Noise level (%)	Crack A (1.00 mm, 0°)	Crack B (0.50 mm, 30°)	Crack C (1.20 mm, 90°)	Crack D (1.20 mm, −70°)
Measured length (mm)	10	1.01 ± 0.12	1.29 ± 3.92	0.24 ± 0.34	2.72 ± 5.12
	20	0.98 ± 0.31	2.29 ± 5.26	2.60 ± 5.61	1.75 ± 4.56
Measured orientation angle (°)	10	−0.05 ± 7.74	32.41 ± 15.05	−4.00 ± 86.32	−23.07 ± 12.61
	20	1.07 ± 10.41	29.00 ± 18.96	−2.32 ± 74.73	−19.25 ± 36.59
Acceptable result rate (%)	10	79	29	0	0
[see (3)]	20	41	14	0	0

$$\mathbf{C} = \frac{1}{M-1}\tilde{\mathbf{L}}\tilde{\mathbf{L}}^{\mathrm{T}}. \tag{5}$$

In (5), $\tilde{\mathbf{L}} \in \mathrm{R}^{N^2 \times M}$, and its column vectors are given by

$$\tilde{\mathbf{l}}_i = \mathbf{l}_i' - \overline{\mathbf{l}}, \quad i = 1, 2, ..., M. \tag{6}$$

Eigendecomposition of $\mathbf{C}$ gives

$$\mathbf{C} = \mathbf{E}\mathbf{D}\mathbf{E}^{\mathrm{T}}, \tag{7}$$

where the ith column of $\mathbf{E}$ is the eigenvector of $\mathbf{C}$, with the corresponding eigenvalue d_i (the ith diagonal element of $\mathbf{D}$). In PCA, most of the information contained in $\mathbf{L}'$ can be reconstructed using only the eigenvectors (principal components) that correspond to the largest eigenvalues [33]. Given a (vectorized) scattering matrix $\mathbf{S}_{\mathrm{n}}$ that contains noise, the projection of $\mathbf{S}_{\mathrm{n}}$ onto the principal components is given by

$$\mathbf{P} = \mathbf{E}_{\mathrm{p}}^{\mathrm{T}}(\mathbf{S}_{\mathrm{n}} - \overline{\mathbf{l}}), \tag{8}$$

where $\mathbf{E}_{\mathrm{p}} \in \mathrm{R}^{N^2 \times k}$ consists of the columns of $\mathbf{E}$ which correspond to the largest k eigenvalues. Then, the denoised version of $\mathbf{S}_{\mathrm{n}}$ is

$$\mathbf{S}_{\mathrm{d}} = \overline{\mathbf{l}} + \mathbf{E}_{\mathrm{p}}\mathbf{P}. \tag{9}$$

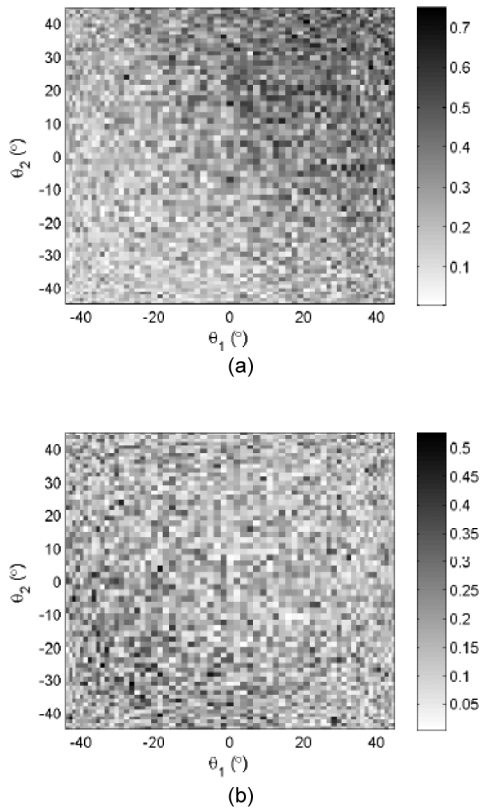

Fig. 5. Scattering matrices of the test cracks with 20% noise [the relative noise level is defined in (2)], where (a) and (b) show the scattering matrices of cracks B and D, respectively.

Regarding the selection of principal components, a commonly used rule of thumb is Kaiser's rule [21], [34], which states that only the principal components with eigenvalues larger than the average eigenvalue should be used for reconstruction. Fig. 6 shows the distribution of the largest 50 eigenvalues calculated from the database, and the first 21 principal components are adopted in this paper according to Kaiser's rule. The denoised versions of the scattering matrices (see Fig. 5) are shown in Figs. 7(a) and 7(b). Again, it is possible to apply HWHM-based characterization to denoised scattering matrices of the test cracks, and the results are specified in Table IV. The measured length and angle in Table IV are calculated from the same 100 realizations of random noise as used in Table III, and also show a spread of two standard deviations from the mean. For crack A, the measurement performance is improved significantly compared with applying HWHM-based characterization directly to the noisy data. Although the acceptable result rate of crack B is decreased because of the systematic error found in the measured orientation angle, the length is measured much more accurately. It is interesting to see that HWHM-based characterization fails for cracks C and D, either because the true peak cannot be identified (for crack C), and/or because multiple peaks are found within the measured angular range (for crack D). Note that most of the noise has been successfully removed in the denoised scattering matrices shown in Figs. 7(a) and 7(b), but there is also a shift in the amplitude compared with those in Fig. 2 (because the scattering matrices of the database cracks are standardized to have zero mean before calculating PCA). To measure the HWHM correctly, this shift is compensated by adding a constant value to the denoised scattering matrices so that the mean of the denoised scattering matrices remain unchanged. However, the mean value of the noise is typically not known *a priori*, so one would have to make an assumption about its

TABLE IV. HWHM-BASED CHARACTERIZATION RESULTS OF CRACKS A–D (DENOISED).

	Noise level (%)	Crack A (1.00 mm, 0°)	Crack B (0.50 mm, 30°)	Crack C (1.20 mm, 90°)	Crack D (1.20 mm, −70°)
Measured length (mm)	10	1.00 ± 0.05	0.42 ± 0.08	NA	NA
	20	0.97 ± 0.06	0.32 ± 0.17	NA	NA
Measured orientation angle (°)	10	−0.06 ± 2.01	35.39 ± 6.41	NA	NA
	20	0 ± 2.01	34.46 ± 8.22	NA	NA
Acceptable result rate (%)	10	100	12	0	0
[see (3)]	20	100	5	0	0

nature. Interestingly, it will be shown that characterization using similarity metrics is invariant to shift, and thus does not require such compensation.

C. The Correlation Coefficient and the Structural Similarity Index as Similarity Metrics

The limitations of the HWHM-based characterization method have been clearly shown in Tables III and IV. When HWHM-based sizing is directly applied to noisy data, the uncertainty in the measurement is extremely high. For the denoised scattering matrices, HWHM-based sizing fails if the specular reflection is not included in the measured angular range (e.g., for test cracks C and D).

Because the original shape of the scattering matrices (see Fig. 2) is recovered very well in the denoised results, the plots of correlation coefficient calculated between the scattering matrices of the reference cracks and the denoised results are visually identical to those shown in Fig. 4. For crack A, the peak is found exactly at the same position as the noise-free case (1 mm, 0°). For cracks C and D, the peaks are found at 1.30 mm, 90° and 1.25 mm, −70°, respectively, without significant change of the landscape. This implies that characterization using the correlation coefficient metric gives acceptable measurement results for cracks A, C, and D.

Fig. 8 shows the distribution of the correlation coefficient calculated for the denoised scattering matrix of crack B, in which a threshold of 0.01 is applied and only the pixel values that are within this threshold from the peak are plotted. It can be seen that the peak is at 0.75 mm, 30°, thus it has a large error (50%) in the measured length. We can also see that besides the global maximum at 0.75 mm, 30° (Peak 1), there is another local maximum at 0.45 mm, 35° (Peak 2) that is near in the value of the correlation coefficient to the global maximum (the values of Peaks 1 and 2 are 0.9928 and 0.9914, respectively). A similar situation occurs for crack D, for which the other local maximum [the flat peak that can be seen from Fig. 4(d)] is located at 1.60 mm, −25°, and has a value (0.9117) near the global maximum (0.9227). Clearly, it is desirable to adopt another similarity metric to distinguish between these competing peaks.

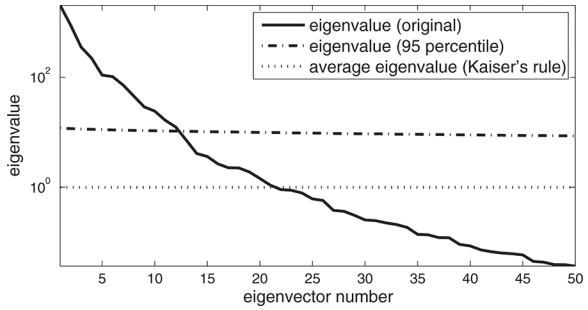

Fig. 6. The first 50 eigenvalues calculated from the database and the 95th percentile calculated from random permutations of the database. Parallel analysis [36] (see the Appendix) suggests use of the first 12 eigenvalues for reconstruction, and the number suggested by Kaiser's rule is 21.

The main problem with the correlation coefficient metric (1) is that when comparing two scattering matrices, features from high-amplitude parts of the scattering matrices dominate the result, and features from low-amplitude parts are less strongly weighted. To address this issue, a second similarity metric, the structural similarity (SSIM) index [35] is introduced, which applies a small local window to images before calculating the local correlation coefficients (so the features in each part of the images are treated equally). In this paper, the structural similarity index is calculated within a 3 × 3 square window. Unlike in the original paper, in which the structural similarity index was calculated based on luminance comparison (i.e., comparing the mean intensities of two images), contrast comparison (comparing the standard deviations of two images), and structure comparison (the correlation coefficient of two images) [35], only the correlation coefficient is calculated here because the other two factors are not invariant to scale and shift. The outcome is the mean SSIM (or MSSIM) index [35], which is the mean of the local correlation coefficients obtained by moving the window pixel-by-pixel over the entire scattering matrices. For scattering matrices $\mathbf{S}_{\mathrm{E}}$ and $\mathbf{S}_{\mathrm{R}}$ (both of size $N \times N$), the MSSIM index is given by

$$\mathrm{MSSIM} = \frac{1}{(N-2)^2}\sum_{i=2}^{N-1}\sum_{j=2}^{N-1}\mathrm{SSIM}(i,j), \tag{10}$$

where $\mathrm{SSIM}(i,j)$ is the correlation coefficient [see (1)] between the 3 × 3 submatrices of $\mathbf{S}_{\mathrm{E}}$ and $\mathbf{S}_{\mathrm{R}}$, which are given by (p = E,R)

$$\tilde{\mathbf{S}}_p = \begin{bmatrix} \mathbf{S}_p(i-1,j-1) & \mathbf{S}_p(i-1,j) & \mathbf{S}_p(i-1,j+1) \\ \mathbf{S}_p(i,j-1) & \mathbf{S}_p(i,j) & \mathbf{S}_p(i,j+1) \\ \mathbf{S}_p(i+1,j-1) & \mathbf{S}_p(i+1,j) & \mathbf{S}_p(i+1,j+1) \end{bmatrix}. \tag{11}$$

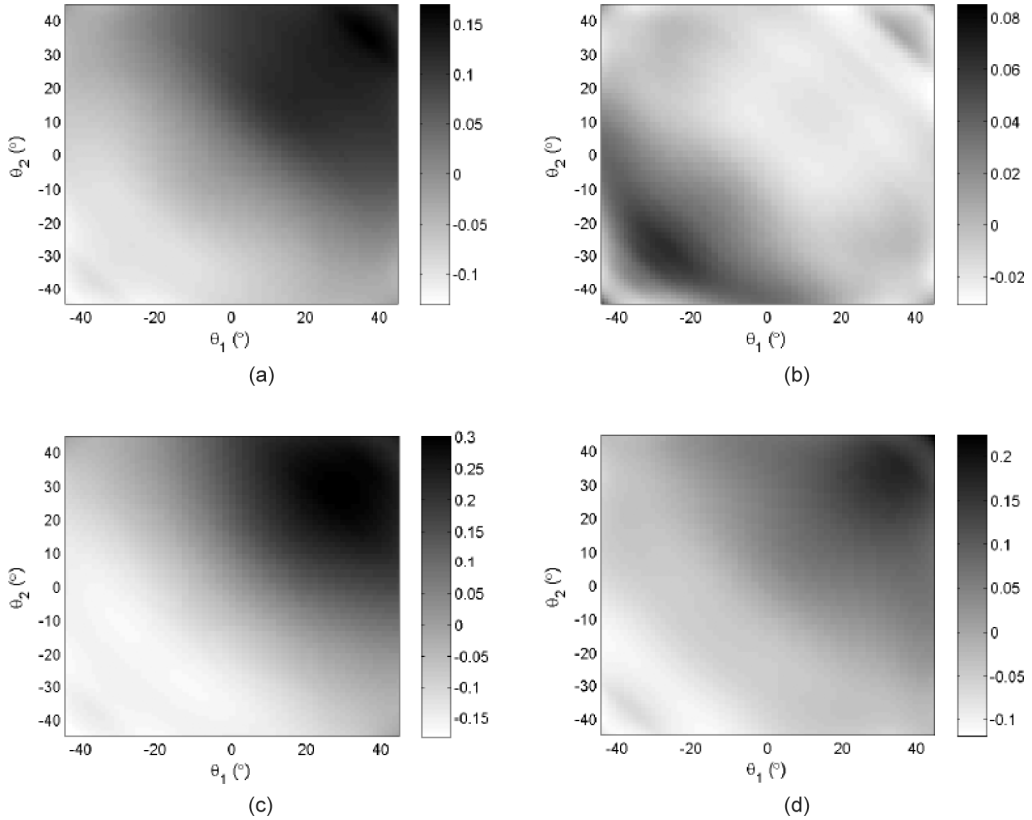

Fig. 7. Scattering matrices of the test cracks (denoised) and two reference cracks found for crack B, where (a) and (b) are the denoised scattering matrices of cracks B and D, respectively, and (c) and (d) are the scattering matrices of two reference cracks (Peak 1: 0.75 mm, 30° and Peak 2: 0.45 mm, 35°) in Fig. 8.

Figs. 7(c) and 7(d) show the scattering matrices represented by Peak 1 (0.75 mm, 30°) and Peak 2 (0.45 mm, 35°) shown in Fig. 8, respectively. Both of them are similar in shape to the denoised scattering matrix of crack B shown in Fig. 7(a), with a difference of 0.0014 in their values of the correlation coefficient. Peak 1 is slightly better than Peak 2 in terms of the correlation coefficient. However, if the MSSIM index is calculated for Peak 1 and Peak 2, they can be distinguished in a clearer way (the MSSIM index of Peak 1 is 0.7449 and Peak 2 is 0.8494). As a result, Peak 2 should be chosen as the match result because it is significantly better than Peak 1 in terms of MSSIM, and it is indeed a better measurement of crack B than Peak 1. Similarly, in the result of crack D, the global peak at 1.25 mm, −70° has a much larger MSSIM index (0.4299) than the flat peak at 1.60 mm, −25° (0.3242) [see Fig. 4(d)], thus it can be regarded as the best match result for this case.

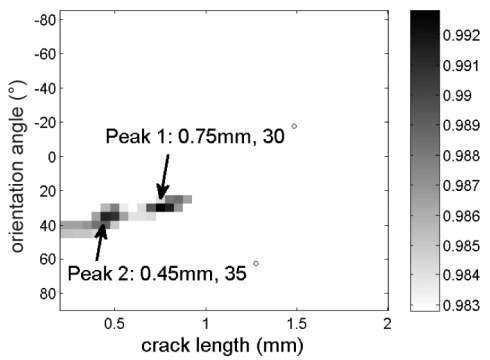

Fig. 8. The correlation coefficients calculated between the scattering matrices of database cracks and crack B (denoised), only showing the peaks and near-peak results with the threshold of 0.01.

In summary, the defect characterization approach proposed in this paper can be described as follows:

- Step 1: Prepare the database, which consists of the scattering matrices of reference cracks. The incident and scattering angles of the scattering matrices should be the same as those of the scattering matrix of the test defect.
- Step 2: Apply PCA to noisy data $\mathbf{S}_{\mathrm{n}}$ to obtain the denoised scattering matrix $\mathbf{S}_{\mathrm{d}}$ [see (8) and (9)]. The number k of principal components that are used for reconstruction can be determined by Kaiser's rule. Alternatively, a proper value for k can be determined by parallel analysis [36] (see the Appendix).
- Step 3: Calculate the correlation coefficients between $\mathbf{S}_{\mathrm{d}}$ and the scattering matrices from the database.
- Step 4: Find peaks (local maxima that have large correlation coefficients) in the preceding result. If an automatic procedure is required, this can be done in iterations, where one peak is found and the peak region (consisting of the peak and the associated near-peak candidates that potentially have large correlation co-

TABLE V. CHARACTERIZATION OF CRACKS A–D WITH NOISE, USING PCA AND SIMILARITY METRICS.

	Noise level (%)	Crack A (1.00 mm, 0°)	Crack B (0.50 mm, 30°)	Crack C (1.20 mm, 90°)	Crack D (1.20 mm, −70°)
Measured length (mm)	10	1.00 ± 0	0.50 ± 0	1.25 ± 0	1.21 ± 0.03
	20	1.00 ± 0	0.50 ± 0.19	1.27 ± 0.05	1.22 ± 0.07
Measured orientation angle (°)	10	0 ± 0	30 ± 0	90 ± 0	−70 ± 0
	20	0 ± 0	34.00 ± 4.92	90 ± 0	−69.10 ± 12.66
Acceptable result rate (%)	10	100	100	100	100
	20	100	88	100	98

efficients) is removed from the result in each iteration. The iteration stops when all of the correlation coefficients above some threshold have been removed. The threshold used to determine the number of peaks must be chosen with care. If the chosen threshold is inappropriate and too many local maxima (most of them are actually false peaks) are found, the MSSIM index can potentially fail to give the desired best match. Although the distribution of the MSSIM index has shaper local peaks than the correlation coefficient, it is globally less robust to changes in the scattering matrix (that are caused by the denoising procedure). For this reason, it is necessary to exclude those less significant peaks by choosing an appropriate threshold, above which the MSSIM index is calculated.

- If there is only one peak in the result obtained at Step 4, the crack is characterized as the corresponding reference crack. If there is more than one peak, the crack is characterized as the one which has the largest MSSIM index.

The proposed approach has been applied to the scattering matrices of test cracks with noise. In the iterative procedure described at Step 4, the peak region is defined as a 0.40 mm × 10° rectangular region with the peak at the center, and the threshold is set to be 0.01 from the maximum correlation coefficient. The noisy data here is the same as that used in Table III, which includes two different noise levels, 10% and 20%, and 100 realizations of random noise for each noise level. As before, the measured length and angle of each test crack and each noise level are given in Table V, showing a spread of two standard deviations from the mean. When the noise level is 10%, the length and orientation angle of cracks A and B are measured to high accuracy for all the cases. There is a constant error in the measured length of crack C (0.05 mm), and a small deviation in the measured length of crack D. However, the angle results are highly accurate for cracks C and D, and the acceptable result rates for all of the test cracks are 100%. When the noise level increases to 20%, the characterization results of crack A are again accurate for all 100 realizations. Although the measured length of crack C shows a small variance, the acceptable result rate of crack C remains 100%. For cracks B and D, incorrect results begin to appear, and specifically, the result of crack B is worse than the other cases. As can be observed from Fig. 4(b), even in the noise-free case, the correlation coefficient peak of crack B has a plateau in both the length and orientation angle axes, which means there are many reference cracks whose scattering matrices are similar in the neighborhood of the peak. It is for this reason that the characterization of small cracks is more easily affected by noise than larger cracks, but the acceptable result rate of crack B would still be satisfactory in many applications. The performance of the algorithm is expected to drop further for smaller cracks, and/or for higher noise levels. Inspection at a higher frequency is expected to be helpful for more accurate characterization of small cracks because this results in further information content in the scattering matrix. For the same reason, adopting an array with a larger aperture size (which extends the angular coverage of the array and the measured scattering matrix) is also expected to be beneficial.

Attempts to characterize non-crack-like defects can be rejected by the described approach, if the calculated correlation coefficients in Step 3 are below some threshold (e.g., 0.9). Fig. 9 shows the correlation coefficients calculated between the scattering matrices of the reference cracks and a 1-mm side-drilled hole. The scattering matrix of a 1-mm hole is calculated using the analytic solution in [37], and reconstructed with $k = 21$ principal components as before. In the result shown in Fig. 9, the peak is located at 1.35 mm, 90°, and the corresponding correlation coefficient is 0.5468, which is significantly lower than the suggested threshold of 0.9. Such a low value is an indication of a poor match, thus none of the reference cracks should be chosen as the match result for the side-drilled hole.

Because real crack-like defects often have rough surface profiles [13], it is important for any characterization approach to be robust to a certain degree of roughness. Given a random surface $z(n)$, its roughness can be described by the rms roughness σ and the correlation length λ_0, which are defined as the standard deviation of $z(n)$, and the distance at which the autocovariance function of $z(n)$ falls by $1/e$ [38], respectively. Figs. 10(a)–10(c) show the profiles of example rough cracks (solid lines) with different roughness parameters. All the cracks have the same length of 1 mm, and they are generated by assuming that the height distribution function and the autocovariance function are Gaussian [38]. The scattering matrices of such rough cracks are calculated using the finite-element local scattering (FELS) model developed in [39]. More details about the rough surface generation and the FELS model can be found in [38].

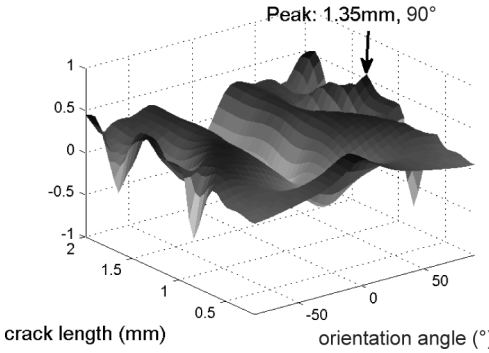

Fig. 9. The correlation coefficients calculated between the scattering matrices of database cracks and a 1-mm side-drilled hole. The peak is located at 1.35 mm, 90°, and the corresponding correlation coefficient is 0.5468.

The performance of the proposed algorithm for the example rough cracks is shown in Fig. 10(a)–10(c), where the dashed lines represent the best match results found for each case. The roughness parameters of the crack shown in Fig. 10(a) are $\sigma = 30$ μm and $\lambda_0 = 50$ μm, and a good match result is found to be 1.10 mm, 0°. The crack shown in Fig. 10(b) has an orientation angle of 45° and similar roughness parameters ($\sigma = 30$ μm, $\lambda_0 = 57$ μm), and is also accurately identified as a 1.10 mm, 40° crack. It can be seen that although the database only consists of scattering matrices of smooth cracks, the performance of the algorithm is still satisfactory for rough cracks, as long as the degradation of the scattering matrix because of roughness is not too severe. In Figs. 10(a) and 10(b), the peak correlation coefficients are 0.9862 and 0.9819 (above the suggested threshold of 0.9), thus both of the characterization results can be safely accepted. However, if the crack shown in Fig. 10(c) ($\sigma = 120$ μm, $\lambda_0 = 43$ μm) is considered, the peak (still plotted and called the best match result) is located at 1.40 mm, 75°, and the corresponding correlation coefficient is 0.8227. For the same reason as for the side-drilled hole, attempts to characterize such cracks with high roughness must be rejected without further calculation of the MSSIM index, because the correlation coefficient falls below the threshold.

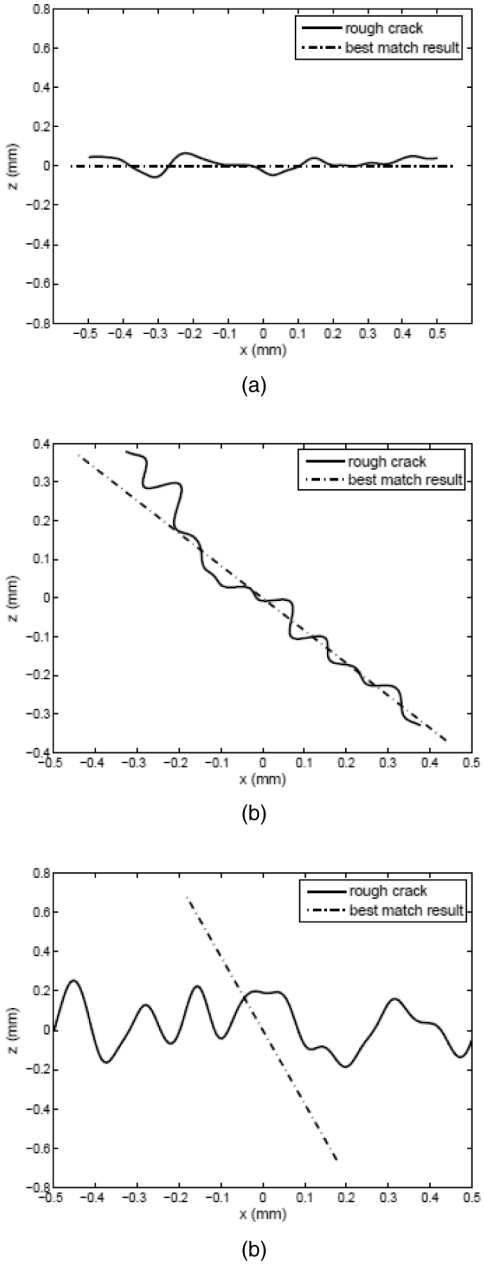

Fig. 10. Surface profiles (solid lines) and the best match results (dashed lines) found with the proposed approach, where the roughness parameters are: (a) $\sigma = 30$ μm, $\lambda_0 = 50$ μm, (b) $\sigma = 30$ μm, $\lambda_0 = 57$ μm, and (c) $\sigma = 120$ μm, $\lambda_0 = 43$ μm. Rough cracks shown in (a) and (b) can be correctly characterized with peak correlation coefficients of 0.9819 and 0.9862; however, the attempt to characterize the rough crack shown in (c) is rejected, because the peak correlation coefficient (0.8227) is below the threshold of 0.9.

IV. Experimental Results

The proposed algorithm has also been studied experimentally. In practice, the scattering matrix of a defect must be extracted from the measured array data; however, the real transmit–receive array data contains a superposition of responses from all scatterers including defects and structural features. The signals from different scatterers are usually overlapped and, in general, it is not possible to isolate and extract the scattered signals from the defect of interest in the original time domain signals. Several signal processing techniques have been developed to extract the scattering matrix from a particular defect from the array data [20], [40]. In the current paper, the subarray approach [20] is used.

A 64-element array with central frequency of 5 MHz (see Table I) was used on an aluminum sample with six scatterers (one 1-mm hole and five 0.25 mm by 1 mm slots with different orientation angles) shown in Fig. 11. The slots were cut using wire electrical discharge machining (EDM), and the detailed machining process and the geometry of the slots can be found in [19]. The scattering matrices of the defects are extracted in separate measurements by moving the array in such a way that the target

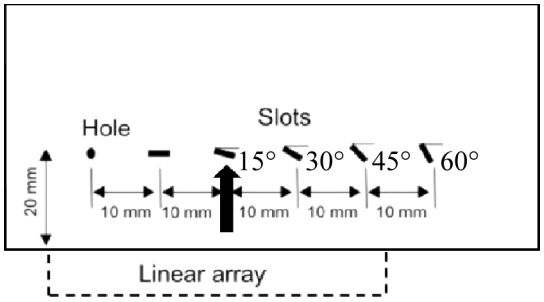

Fig. 11. Experimental measurements of the scattering matrices. The 15° slot is at the array center in the figure, and its scattering matrix is extracted from the array data. For the measurement of the 60° slot and 1-mm hole, the array is moved to the right-hand edge and left-hand edge of the sample, respectively.

defect is located at the array center (this is the same as the test geometry shown in Fig. 1). In Fig. 11, the 15° slot is at the array center, and its scattering matrix is extracted from the array data. The scattering matrices of the 0°, 30°, and 45° slots are extracted in the same manner. For the measurement of the 60° slot, the array is moved to the right-hand edge of the sample, but the target defect is not exactly at the array center. Similarly, the scattering matrix of the 1-mm hole is measured by placing the array at the left-hand edge.

Figs. 12(a)–12(f) show the extracted scattering matrices of the 1-mm hole and the slots of orientation angles 0°, 15°, 30°, 45°, and 60°, respectively. Note that the subarray approach adopted to extract scattering matrices suffers from a small amount of interference from nearby defects [the interference can be seen as diagonal stripes in Figs. 12(a)–12(c)]. Given the different array–defect configurations, three different databases are needed for the characterization of the 1-mm hole, the 60° slot, and the four inner slots.

The proposed algorithm is applied to the scattering matrices shown in Fig. 12. For each case, the number of principal components k is selected by both Kaiser's rule and parallel analysis (see the Appendix), and their performance is compared. Before performing PCA, both the scattering matrices of reference cracks and those extracted experimentally are normalized to their maximum amplitudes. This is necessary because otherwise the experimentally measured scattering matrices as shown in Fig. 12 cannot be effectively centered by subtracting the mean [see (8)] which is obtained from the scattering matrices of reference cracks. The normalization of the scattering matrices in this manner does not change the shape, and the match results are not affected. It is also much easier than the calibration of experimental data, which requires measurements from a reference defect. The characterization results are tabulated in Table VI. As in the simulation case, the peak is found at 1.35 mm, 90° (when $k =$ 9 and 17) for the 1-mm hole, but the results should be rejected because of the low values of the correlation coefficient (0.6538 when $k = 9$ and 0.6739 when $k = 17$). For the slots, the selection of k by both suggested methods performs equally well. The measured orientation angles are in excellent agreement with the actual values, and the errors in the measured length are within 0.10 mm. It should be pointed out that within the angular ranges shown in Figs. 12(b)–12(f), there is no significant difference between the scattering matrices of the slots and their ideal counterparts (reference cracks of the same size and orientation angle). As a result, the measurement results given by the proposed algorithm are reliable. However, if the experimentally extracted scattering matrix only consists of the tip-diffracted signal from the machined slots, performance degradation of the algorithm could be expected.

V. Conclusions

An approach for the characterization of small cracks has been proposed. The scattering matrix of test defects is denoised by the application of principal component analysis. When the noise in the data is considerable, the number of principal components used for reconstruction should be carefully chosen, and this can be achieved by using Kaiser's rule or through parallel analysis (see the Appendix). In addition, when the test defect falls outside the database, the peak correlation coefficient found with the database cracks was below a threshold, and such results could be rejected because they indicate poor matches with the reference cracks.

The correlation coefficient and the structural similarity index are used as the similarity measures. With the correlation coefficient metric, some candidate cracks are chosen, which are distinguished at the next step by calculating the mean structural similarity index. If an automatic procedure is required, the peaks can be found in the iterative procedure described in Section III-C. In this paper, all of the simulation and experimental results of the proposed algorithm are obtained using this automatic procedure. When the noise level is low, the acceptable result rates of all the test cracks in the simulation case are 100%, and the results of five experimentally measured subwavelength cracks are also acceptable (the errors in the measured length and orientation angle are within 0.10 mm and 5°). The measurement becomes less accurate as the noise level increases, but the acceptable result rate is 88% even for the smallest crack (crack B), which has a size of less than half a wavelength.

Appendix

In principal component analysis, the selection of the number of principal components is regarded as one of the major difficulties [41]. Increasing the number of principal components is always beneficial for the reconstruction of database cracks (i.e., scattering matrices without noise). However, if the scattering matrix contains noise, and PCA is adopted for denoising purposes, using too many principal components will also allow much of the noise to be

TABLE VI. CHARACTERIZATION OF SIX TEST SCATTERERS SHOWN IN FIG. 11.

	Number of principal components k	Characterization result	Peak correlation coefficient
1 mm hole	17 (Kaiser's rule)	1.35 mm, 60°	0.6739
	9 (parallel analysis)	1.35 mm, 60°	0.6538
1 mm, 0° crack	18 (Kaiser's rule)	1.00 mm, 0°	0.9732
	10 (parallel analysis)	0.95 mm, 0°	0.9758
1 mm, 15° crack	18 (Kaiser's rule)	1.05 mm, 15°	0.9852
	10 (parallel analysis)	1.05 mm, 15°	0.9842
1 mm, 30° crack	18 (Kaiser's rule)	1.10 mm, 30°	0.9908
	10 (parallel analysis)	1.10 mm, 30°	0.9867
1 mm, 45° crack	18 (Kaiser's rule)	1.10 mm, 45°	0.9748
	10 (parallel analysis)	1.05 mm, 45°	0.9653
1 mm, 60°	17 (Kaiser's rule)	1.10 mm, 60°	0.9885
	9 (parallel analysis)	1.10 mm, 60°	0.9734

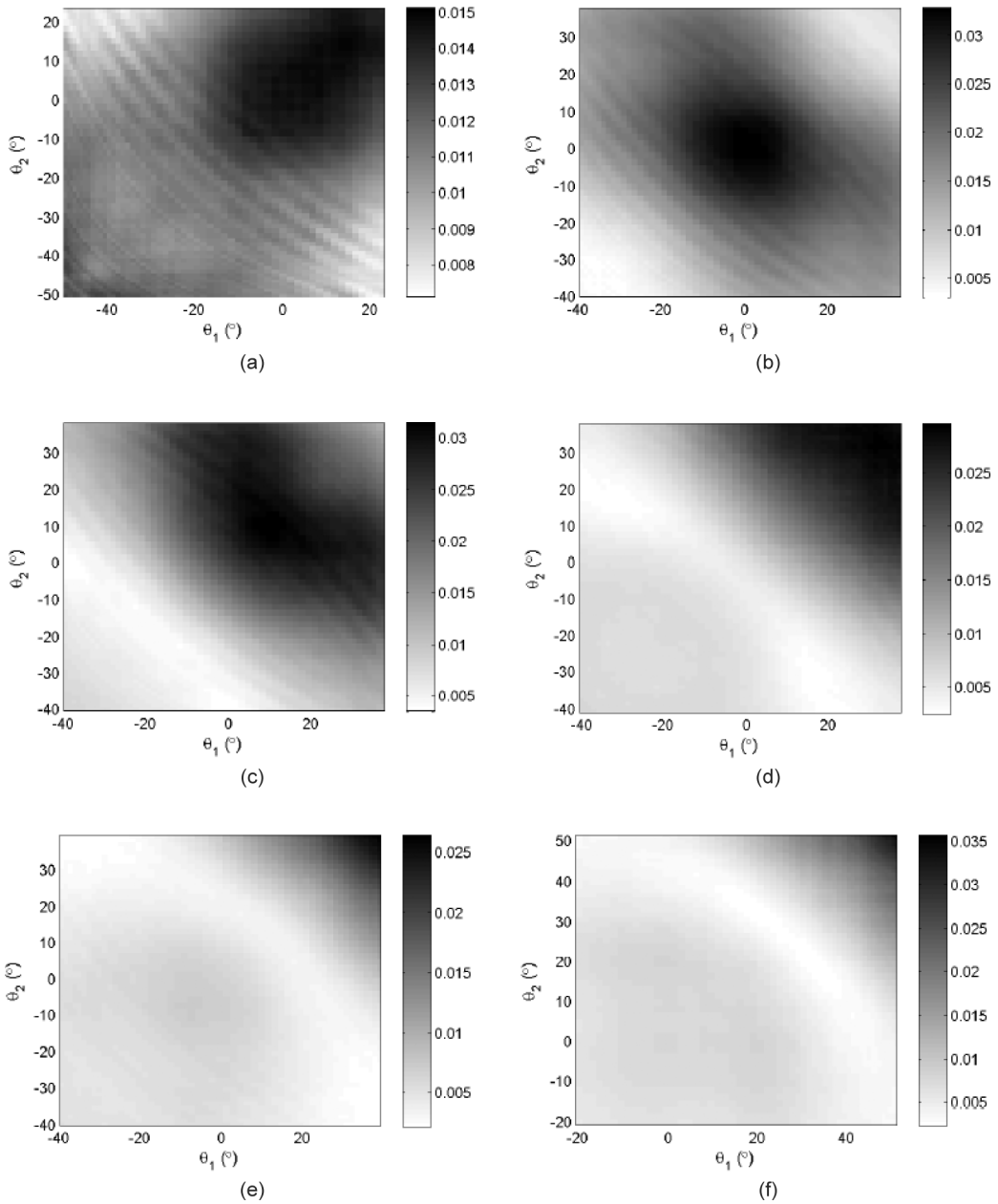

Fig. 12. The experimentally extracted scattering matrices of the six scatterers, where (a)–(f) are the scattering matrices of the 1-mm hole and the slots of orientation angles 0°, 15°, 30°, 45°, and 60°, respectively. A subarray approach [20] is used to extract the scattering matrices from the array data.

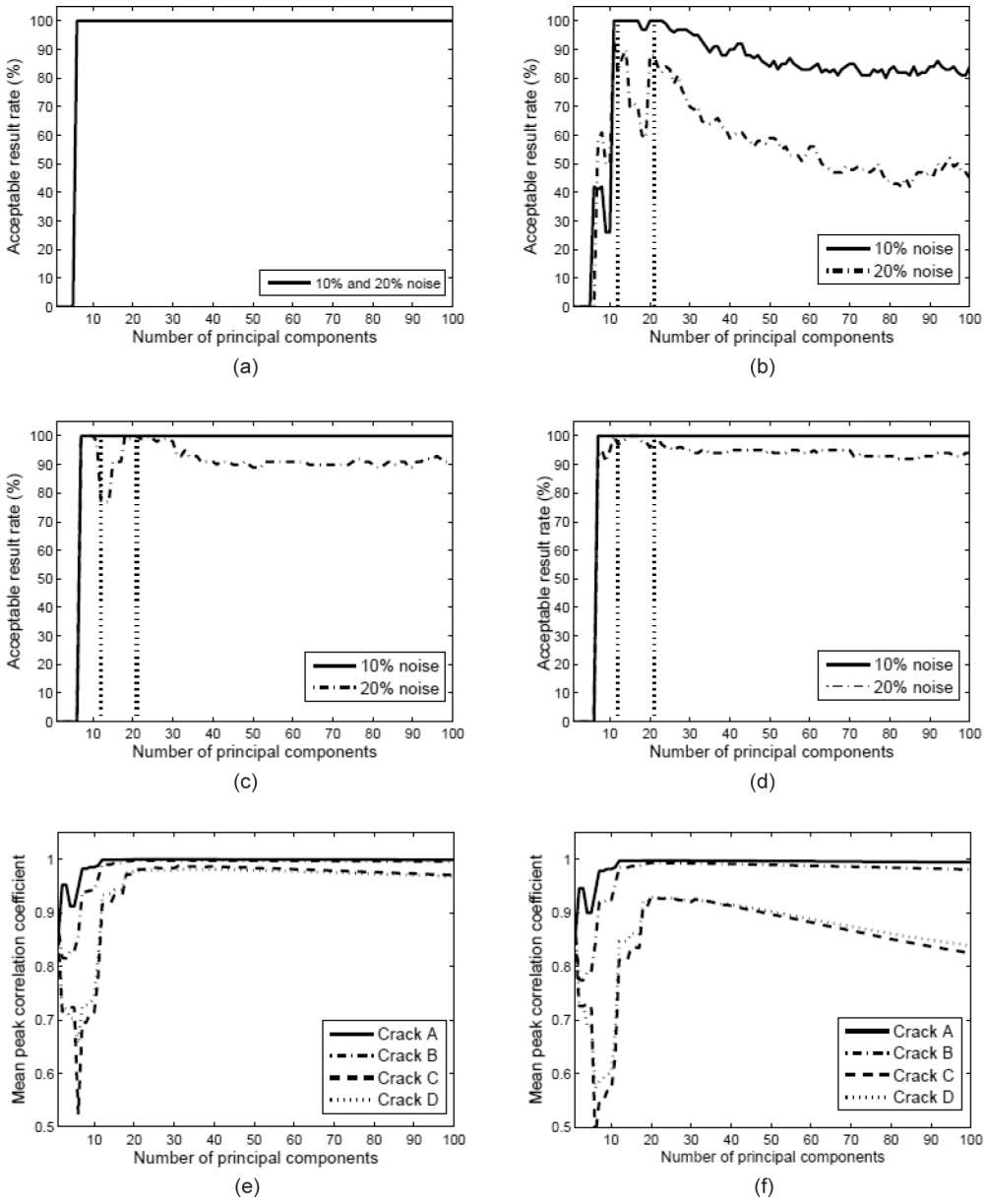

Fig. 13. Characterization results of the proposed algorithm with different number of principal components, where (a)–(d) show the acceptable result rates of cracks A–D with noise, and (e) and (f) show the mean peak correlation coefficients when the noise level is 10% and 20%, respectively. $k = 21$ corresponds to Kaiser's rule, and $k = 12$ is the result of parallel analysis.

included in the reconstructed version (the model is said to be overparameterized [41]). According to Kaiser's rule, for the noisy data in this paper, the first 21 principal components are selected, and the characterization results using similarity metrics based on the denoised scattering matrices are satisfactory, as shown in Table V. The effect of the number of the principal components on the characterization result is shown in Fig. 13. For a given number of principal components k, the first k principal components are used to reconstruct the scattering matrices, and the algorithm proposed in Section III-C is adopted for the denoised scattering matrices. Figs. 13(a)–13(d) show the acceptable result rates of cracks A–D as a function of k (the same 100 realizations of noise as in Table V are used), and Figs. 13(e)–13(f) show the change of the mean peak correlation coefficients when the noise level is 10% and 20%, respectively. When the noise level is 10%, the acceptable result rates for cracks A, C, and D remain 100% as long as k is larger than 6, which means the reconstruction is not affected significantly by increasing k. This can also be seen from Fig. 13(e), where the peak correlation coefficients do not fall after reaching maximum at approximately $k = 20$. On the other hand, the acceptable result rates of cracks C and D decreases (while crack A is still not affected) after achieving maximum when the noise level is 20%, which suggests that the reconstruction becomes degraded as k further increases. This can also be confirmed by the peak correlation coefficients shown in Fig. 13(f). The result is similar for crack B, except that the acceptable result rate diminishes after reaching maximum for both 10% and 20%

noise. For all of the cases shown in Fig. 13(a)–13(d), $k = 21$ which is obtained by Kaiser's rule proves to be a good choice for the number of principal components to retain.

The number of principal components k can also be determined from parallel analysis [36]. In parallel analysis, the eigenvalues obtained by applying PCA to the database are compared with those obtained by applying PCA to a set of uncorrelated data matrices that have the same size as the database [41]. Uncorrelated data matrices are obtained by random permutations of the data as is suggested in [42], and PCA is applied to 100 such randomized matrices to calculate the 95th percentile of the distribution of the eigenvalues [21]. The result is shown in Fig. 6, and the suggested value of k by parallel analysis is 12. It can be seen from Fig. 13 that the results obtained when $k = 12$ are also satisfactory (but when k lies between 12 and 21, the acceptable result rate decreases when the noise level is 20%). The only exception is found for crack C, but this can be predicted by the low value of the peak correlation coefficient when $k = 12$ [see Fig. 13(f)].

References

[1] J. D. Achenbach, "Quantitative nondestructive evaluation," *Int. J. Solids Struct.*, vol. 37, no. 1–2, pp. 13–27, 2000.

[2] I. Komura, T. Hirasawa, S. Nagai, J. Takabayashi, and K. Naruse, "Crack detection and sizing technique by ultrasonic and electromagnetic methods," *Nucl. Eng. Des.*, vol. 206, no. 2–3, pp. 351–362, 2001.

[3] R. Demirli and J. Saniie, "Model-based estimation of ultrasonic echoes. Part I: Analysis and algorithms," *IEEE Trans. Ultrason. Ferroelectr. Freq. Control*, vol. 48, no. 3, pp. 787–802, 2001.

[4] L. Satyanarayan, K. Bharath Kumaran, C. V. Krishnamurthy, and K. Balasubramaniam, "Inverse method for detection and sizing of cracks in thin sections using a hybrid genetic algorithm based signal parametrisation," *Theor. Appl. Fract. Mech.*, vol. 49, no. 2, pp. 185–198, 2008.

[5] B. Shakibi, F. Honarvar, M. D. C. Moles, J. Caldwell, and A. N. Sinclair, "Resolution enhancement of ultrasonic defect signals for crack sizing," *NDT & E Int.*, vol. 52, pp. 37–50, Nov. 2012.

[6] B. W. Drinkwater and P. D. Wilcox, "Ultrasonic arrays for nondestructive evaluation: A reivew," *NDT & E Int.*, vol. 39, no. 7, pp. 525–541, 2006.

[7] C. Holmes, B. W. Drinkwater, and P. D. Wilcox, "Post-processing of the full matrix of ultrasonic transmit-receive array data for nondestructive evaluation," *NDT & E Int.*, vol. 38, no. 8, pp. 701–711, 2005.

[8] M. G. Lozev, R. L. Spencer, and D. Hodgkinson, "Optimized inspection of thin-walled pipe welds using advanced ultrasonic techniques," *J. Pressure Vessel Technol.*, vol. 127, no. 3, pp. 237–243, 2005.

[9] S. Mahaut, O. Roy, C. Beroni, and B. Rotter, "Development of phased array techniques to improve characterization of defect located in a component of complex geometry," *Ultrasonics*, vol. 40, no. 1–8, pp. 165–169, 2002.

[10] N. Pörtzgen, D. Gisolf, and G. Blacquiere, "Inverse wave field extrapolation: A different NDI approach to imaging defects," *IEEE Trans. Ultrason. Ferroelectr. Freq. Control*, vol. 54, no. 1, pp. 118–127, 2007.

[11] A. J. Hunter, B. W. Drinkwater, and P. D. Wilcox, "The wavenumber algorithm for full-matrix imaging using an ultrasonic array," *IEEE Trans. Ultrason. Ferroelectr. Freq. Control*, vol. 55, no. 11, pp. 2450–2462, 2008.

[12] J. Zhang, B. W. Drinkwater, and P. D. Wilcox, "The use of ultrasonic arrays to characterise crack-like defects," *J. Nondestruct. Eval.*, vol. 29, no. 4, pp. 222–232, 2010.

[13] J. Zhang, B. W. Drinkwater, and P. D. Wilcox, "Effect of roughness on imaging and sizing rough crack-like defects using ultrasonic arrays," *IEEE Trans. Ultrason. Ferroelectr. Freq. Control*, vol. 59, no. 5, pp. 939–948, 2012.

[14] L. Adler and J. D. Achenbach, "Elastic wave diffraction by elliptical cracks: Theory and experiment," *J. Nondestruct. Eval.*, vol. 1, no. 2, pp. 87–99, 1980.

[15] R. K. Chapman, "A system model for the ultrasonic inspection of smooth planar cracks," *J. Nondestruct. Eval.*, vol. 9, no. 2–3, pp. 197–210, 1990.

[16] A. Bostrom and H. Wirdelius, "Ultrasonic probe modeling and nondestructive crack detection," *J. Acoust. Soc. Am.*, vol. 97, no. 5, pp. 2836–2848, 1995.

[17] P. Bovic and A. Bostrom, "A model of ultrasonic nondestuctive testing for internal and sub-surface cracks," *J. Acoust. Soc. Am.*, vol. 102, no. 5, pp. 2723–2733, 1997.

[18] A. L. Lopez-Sanchez, H. J. Kim, L. W. Schmerr, and A. Sedov, "Measurement models and scattering models for predicting the ultrasonic pulse-echo response from side-drilled holes," *J. Nondestruct. Eval.*, vol. 24, no. 3, pp. 83–96, 2005.

[19] P. D. Wilcox, C. Holmes, and B. W. Drinkwater, "Advanced reflector characterisation with ultrasonic phased arrays in NDE applications," *IEEE Trans. Ultrason. Ferroelectr. Freq. Control*, vol. 54, no. 8, pp. 1541–1550, 2007.

[20] J. Zhang, B. W. Drinkwater, and P. D. Wilcox, "Defect characterization using an ultrasonic array to measure the scattering coefficient matrix," *IEEE Trans. Ultrason. Ferroelectr. Freq. Control*, vol. 55, no. 10, pp. 2254–2265, 2008.

[21] I. T. Jolliffe, *Principal Component Analysis*, 2nd ed., New York, NY: Springer-Verlag, 2002.

[22] E. Glushkov, N. Glushkova, A. Ekhlakov, and E. Shapar, "An analytically based computer model for surface measurements in ultrasonic crack detection," *Wave Motion*, vol. 43, no. 6, pp. 458–473, 2006.

[23] L. W. Schmerr, *Fundamentals of Ultrasonic NonDestructive Evaluation: A Modeling Approach*. New York, NY: Plenum, 1998.

[24] A. A. Goshtasby, *2-D and 3-D Image Registration for Medical, Remote Sensing, and Industrial Applications*. Hoboken, NJ: Wiley-Interscience, 2005.

[25] A. A. Goshtasby, *Image Registration: Principles, Tools and Methods*. London, UK: Springer-Verlag, 2012.

[26] K. Pearson, "Contributions to the mathematical theory of evolution—III. Regression, heredity, and panmixia," *Philos. Trans. R. Soc. Lond. A*, vol. 187, pp. 253–318, 1896.

[27] C. Spearman, "The proof and measurement of association between two things," *Am. J. Psychol.*, vol. 15, no. 1, pp. 72–101, 1904.

[28] M. G. Kendall, "A new measure of rank correlation," *Biometrika*, vol. 30, no. 1–2, pp. 81–93, 1938.

[29] P. Viola and W. M. Wells III, "Alignment by maximization of mutual information," *Int. J. Comput. Vis.*, vol. 24, no. 2, pp. 137–154, 1997.

[30] J. Kim, "Intensity based image registration using robust similarity measure and constrained optimization: Applications for radiation therapy," Ph.D. thesis, Dept. Electr. Eng., University of Michigan, Ann Arbor, MI, 2004.

[31] B. Zitova and J. Flusser, "Image registration methods: A survey," *Image Vis. Comput.*, vol. 21, no. 11, pp. 977–1000, 2003.

[32] A. Sotiras, C. Davatzikos, and N. Paragios, "Deformable medical image registration: A survey," *IEEE Trans. Med. Imaging*, vol. 32, no. 7, pp. 1153–1190, 2013.

[33] M. Turk and A. Pentland, "Eigenfaces for recognition," *J. Cogn. Neurosci.*, vol. 3, no. 1, pp. 71–86, 1991.

[34] H. F. Kaiser, "The application of electronic computers to factor analysis," *Educ. Psychol. Meas.*, vol. 20, pp. 141–151, 1960.

[35] Z. Wang, A. C. Bovik, H. R. Sheikh, and E. P. Simoncelli, "Image quality assessment: From error visibility to structural similarity," *IEEE Trans. Image Process.*, vol. 13, no. 4, pp. 600–612, 2004.

[36] J. L. Horn, "A rationale and test for the number of factors in factor analysis," *Psychometrika*, vol. 30, no. 2, pp. 179–185, 1965.

[37] R. J. Brind, J. D. Achenbach, and J. E. Gubernatis, "High-frequency scattering of elastic waves from cylindrical cavities," *Wave Motion*, vol. 6, no. 1, pp. 41–60, 1984.

[38] J. Zhang, B. W. Drinkwater, and P. D. Wilcox, "Longitudinal wave scattering from rough crack-like defects," *IEEE Trans. Ultrason. Ferroelectr. Freq. Control*, vol. 58, no. 10, pp. 2171–2180, 2011.

[39] A. Velichko and P. D. Wilcox, "A generalized approach for efficient finite element modelling of elastodynamic scattering in two and three dimensions," *J. Acoust. Soc. Am.*, vol. 128, no. 3, pp. 1004–1014, 2010.

[40] A. Velichko and P. D. Wilcox, "Reversible back-propagation imaging algorithm for postprocessing of ultrasonic array data," *IEEE Trans. Ultrason. Ferroelectr. Freq. Control*, vol. 56, no. 11, pp. 2492–2503, 2009.
[41] S. Valle, W. Li, and S. J. Qin, "Selection of the number of principal components: The variance of the reconstruction error criterion with a comparison to other methods," *Ind. Eng. Chem. Res.*, vol. 38, no. 11, pp. 4389–4401, 1999.
[42] A. Buja and N. Eyuboglu, "Remarks on parallel analysis," *Multivariate Behav. Res.*, vol. 27, no. 4, pp. 509–540, 1992.

Long Bai was born in Yanji, P.R. China, in 1987. He received a B.Sc. degree in electronic and information science and technology, and an M.Eng. degree in dynamical systems and control from Peking University, P.R. China, in 2010 and 2013, respectively. Since 2013, he has been a Ph.D. student in the Ultrasonic and NDT group at the University of Bristol, and is currently working on defect characterization using ultrasonic arrays for NDE applications.

Alexander Velichko was born in Krasnodar, Russia, in 1975. He received the M.Sc. degree in applied mathematics from the Kuban State University, Krasnodar, Russia, in 1998, and the Ph.D. degree from the Rostov State University, Rostov-on-Don, Russia, in 2002. His doctoral research was on investigation of wave fields caused by internal vibration sources in layered elastic medium.

From 2005 to 2012, he was employed as a research associate in the Ultrasonics and Nondestructive Testing Research Group at the University of Bristol. In 2012, he was appointed as a lecturer in the Department of Mechanical Engineering at the University of Bristol, England. His current research interests include mathematical modeling of propagation and scattering of elastic waves, ultrasonic imaging using arrays, and guided waves and signal processing.

Bruce W. Drinkwater was born in Hexham, England, in 1970. He received B.Eng. and Ph.D. degrees in mechanical engineering from Imperial College, London, England, in 1991 and 1995 respectively. His Ph.D. thesis was on the subject of solid coupled ultrasonic devices for nondestructive evaluation.

Since 1996, he has worked as an academic in the Mechanical Engineering Department at the University of Bristol, England. He was promoted to Professor in 2007. His research interests focus on ultrasonics and NDE. He has published more than 100 journal articles covering 1) the interaction of ultrasound with adhesive joints, thin layers, and interfaces, 2) ultrasonic array imaging for NDE, and 3) acoustic radiation force devices for particle manipulation applications in biology and materials engineering.

Between 2000 and 2005, he was an EPSRC Advanced Research Fellow, and in 2010, he received the Roy Shape Prize for his significant contribution to NDE research.